ChemInform Abstract: Design, Synthesis, Docking Study and Biological Evaluation of Some Novel Tetrahydrochromeno [3′,4′:5,6]Pyrano[2,3-b]quinolin-6(7H)-one Derivatives Against Acet…

ARTICLE *in* EUROPEAN JOURNAL OF MEDICINAL CHEMISTRY · AUGUST 2013

Impact Factor: 3.45 · DOI: 10.1016/j.ejmech.2013.07.045 · Source: PubMed

9 AUTHORS, INCLUDING:

Mehdi Khoobi
Tehran University of Medical Sciences

Amirhossein Sakhteman
University of Eastern Finland

Hamid Nadri
Shahid Sadoughi University of Medical Scie…

Alireza Foroumadi
Tehran University of Medical Sciences

European Journal of Medicinal Chemistry 68 (2013) 260–269

Contents lists available at ScienceDirect

European Journal of Medicinal Chemistry

journal homepage: http://www.elsevier.com/locate/ejmech

Original article

Design, synthesis, biological evaluation and docking study of 5-oxo-4,5-dihydropyrano[3,2-*c*]chromene derivatives as acetylcholinesterase and butyrylcholinesterase inhibitors

Mehdi Khoobi [a], Masoumeh Alipour [b], Amirhossein Sakhteman [c], Hamid Nadri [c], Alireza Moradi [c], Mehdi Ghandi [b], Saeed Emami [d], Alireza Foroumadi [a,e], Abbas Shafiee [a,*]

[a] Department of Medicinal Chemistry, Faculty of Pharmacy and Pharmaceutical Sciences Research Center, Tehran University of Medical Sciences, Tehran 14176, Iran
[b] School of Chemistry, University College of Science, University of Tehran, PO Box 14155-6455, Tehran, Iran
[c] Faculty of Pharmacy, Shahid Sadoughi University of Medical Sciences, Yazd, Iran
[d] Department of Medicinal Chemistry and Pharmaceutical Sciences Research Center, Faculty of Pharmacy, Mazandaran University of Medical Sciences, Sari, Iran
[e] Neuroscience Research Center, Kerman University of Medical Sciences, Kerman, Iran

ARTICLE INFO

Article history:
Received 3 May 2013
Received in revised form
12 July 2013
Accepted 14 July 2013
Available online 11 August 2013

Keywords:
Alzheimer's disease
Acetylcholinesterase
Chromenes
Coumarins
Docking study

ABSTRACT

A series of fused coumarins namely 5-oxo-4,5-dihydropyrano[3,2-*c*]chromenes linked to *N*-benzylpyridinium scaffold were synthesized and evaluated as acetylcholinesterase (AChE) and butyrylcholinesterase (BuChE) inhibitors. The 1-(4-fluorobenzyl)pyridinium derivative **6g** showed the most potent anti-AChE activity (IC_{50} value = 0.038 μM) and the highest AChE/BuChE selectivity (SI > 48). The docking study permitted us to rationalize the observed structure–affinity relationships and to detect possible binding modes.

1. Introduction

Alzheimer's disease (AD) is the most common cause of dementia among the elderly patients, which leads to progressive decline in cognition and memory [1]. This neurological disorder characterized by reducing levels of acetylcholine (ACh) in the cortex and hippocampus regions of brain [2]. However, the pathogenesis of AD is highly complicated, and the low levels of acetylcholine also associated with the presence of numerous plaques of amyloid β-peptide (Aβ), neurofibrillary tangles and oxidative stress [3,4].

Acetylcholine is primarily hydrolyzed by acetylcholinesterase (AChE) enzyme, and terminated its action. Thus, one of the most promising approaches adopted for palliative treatment of AD is the increasing of acetylcholine levels in the brain by targeting the AChE enzyme [5]. Recently, it has been reported that in AD patients, AChE activity is greatly reduced in specific regions of the brain while butyrylcholinesterase (BuChE) activity increases, likely as compensation for AChE decrease. Due to the key role of BuChE in hydrolysis of ACh, preserving the AChE/BuChE activity ratios in damaged brain is essential for successful treatment of AD. Thus, dual inhibition of AChE and BuChE might improve the signs and symptoms in AD patients [6].

Several AChE inhibitors (Fig. 1) such as rivastigmine, donepezil, galantamine, and tacrine are the main agents for the improvement of cognitive function and the enhancement of memory in AD patients [7,8]. Moreover, several studies have also suggested that AChE inhibitors interfere with the synthesis, deposition and aggregation of Aβ [9,10]. Molecular study evidences have shown that the interaction of some AChE inhibitors with the peripheral anionic site (PAS) of AChE may be involved in Aβ deposition [11,12]. Indeed, the PAS and catalytic site (CS) of AChE enzyme are characterized by two tryptophan residues located at the entrance and the bottom of the active-site gorge. Based on the dual binding model with the

* Corresponding author. Tel.: +98 21 66406757; fax: +98 21 66461178.
E-mail address: ashafiee@ams.ac.ir (A. Shafiee).

0223-5234/$ – see front matter © 2013 Elsevier Masson SAS. All rights reserved.
http://dx.doi.org/10.1016/j.ejmech.2013.07.038

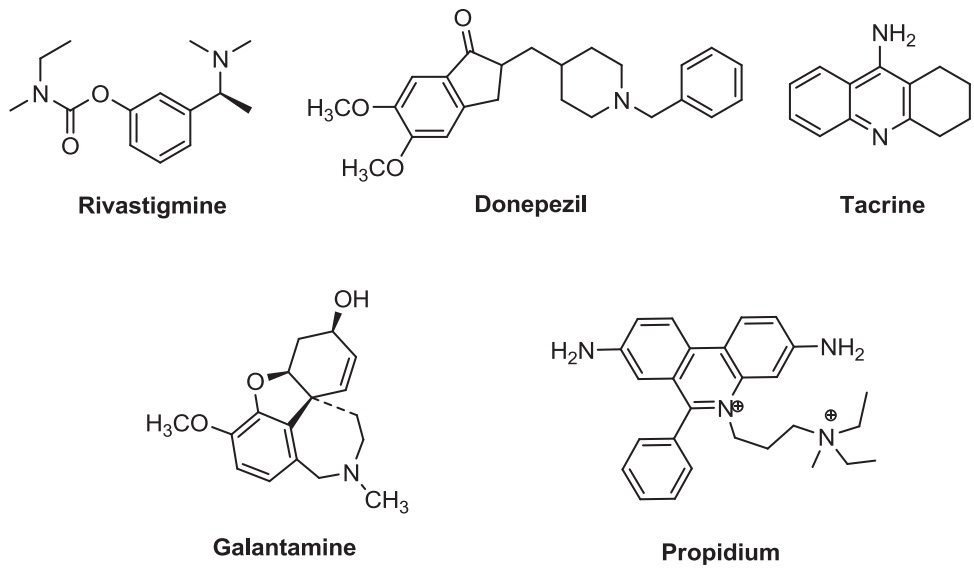

Fig. 1. Structures of well known AChE inhibitors.

AChE, compounds that interact with both CS and PAS could be effective agents for the management of AD [10,13].

A structural survey of AChE inhibitors revealed that AP2238 and ensaculin have a distinct scaffold with a coumarin moiety (Fig. 2). Moreover, a number of naturally occurring and synthetic coumarin analogs exhibited potent AChE inhibitory activity [14]. It has been demonstrated that AChE inhibitors with coumarin moiety primarily interact with the PAS of AChE [15,16]. These findings prompt medicinal chemists to design dual inhibitors of AChE by incorporating a catalytic site interacting moiety with coumarin through an appropriate linker [14].

In this regard, we have previously designed a series of coumarin and coumaranone AChE inhibitors linked to benzyl pyridinium group (Fig. 2) with the capability of interaction with both sites of the enzyme [17]. In continuation of our study of developing new AChE inhibitors, in this work we synthesized a series of fused coumarins **6a**–**o** namely 5-oxo-4,5-dihydropyrano[3,2-*c*]chromene derivatives linked to *N*-benzylpyridinium scaffold and evaluated them as AChE and BuChE inhibitors.

2. Chemistry

In this work, we describe synthesis of a novel series of pyranochromenes **6a**–**o** bearing an *N*-benzylpyridinium moiety in a rather convenient way, owing to the good accessibility of the pyranochromenes nucleus. As outlined in Scheme 1, these compounds could be easily prepared by the simple treatment of 2-amino-5-oxo-4-(pyridin-3 or 4-yl)-4,5-dihydropyrano[3,2-c]chromene-3-carbonitriles **5a**, **b** with different benzyl chlorides. Several methods have been reported for the synthesis of dihydropyrano[*c*]chromenes. Recently, a green inorganic–organic hybrid magnetic nanocatalyst in aqueous medium was used successfully for the synthesis of 2-amino-5-oxo-4,5-dihydropyrano[3,2-*c*]chromene-3-carbonitriles [18]. Accordingly, compounds **5** were synthesized using a commercial pyridine-3 or 4-carbaldehydes (**1a** or **1b**) and malononitrile (**2**) and subsequent reaction with 4-hydroxycoumarin (**4**) in the presence of catalytic amount of magnetic nanocatalyst. The target compounds **6** were prepared through the reaction of compounds **5** with benzyl chlorides having electron donating or withdrawing substitutions, in dry acetonitrile under reflux condition. On cooling, the precipitate was filtered and washed with diethyl ether. The notable features of this method are the easy product isolation with high yields without application of column chromatography.

3. Results and discussion

3.1. In vitro inhibition of AChE and BuChE

The target compounds **6a**–**o** were evaluated for their in vitro inhibitory activities against AChE and BuChE in comparison with marketed AChE inhibitor donepezil as standard drug. The anticholinesterase activities (μM) of two series of compounds 4-pyridinium and 3-pyridinium derivatives (**6a**–**i** and **6j**–**o**, respectively) are shown in Table 1. The data are expressed as mean ± S.E. of three independent experiments. The data were statistically analyzed by means of one-way ANOVA (Analysis of Variance) followed by Newman–Kules post-test to compare each pair of the compounds (P values < 0.05 were considered as significant).

The IC_{50} values of test compounds demonstrated that all compounds showed significant inhibition against AChE at concentrations less than 7.5 μM. The most active compounds were 4-fluoro- and 3,4-dichloro-analogs of 4-pyridinium series (compounds **6g** and **6h**) with IC_{50} values $\leq$ 0.044 μM. Furthermore, compounds **6f**, **6i** and **6n** exhibited good anti-AChE activity (IC_{50} values = 0.48–0.831 μM). Although, compounds **6g**–**i** were also the most active compounds toward BuChE (IC_{50} values = 0.566–1.84 μM) but the selectivity of compounds **6g** and **6h** for AChE was higher than 28. In contrast, compound **6i** with high anticholinesterase activity showed no significant selectivity for AChE/BuChE. In general, the anti-AChE activities of all compounds with the exception of **6i** and **6o** were about 3–48 times more than their anti-BuChE activities.

3.2. Structure–activity relationships

The inhibitory activity of 4-pyridinium derivatives **6a**–**i** against AChE demonstrated that *para*-fluoro derivative **6g** showed the most potent activity, while *ortho*- or *meta*-flouro derivatives (**6a** and **6d**) were less active halo-substituted compounds. Moreover, the introduction of 3-chloro, 3,4-dichoro or 2,4-dichloro on *N*-

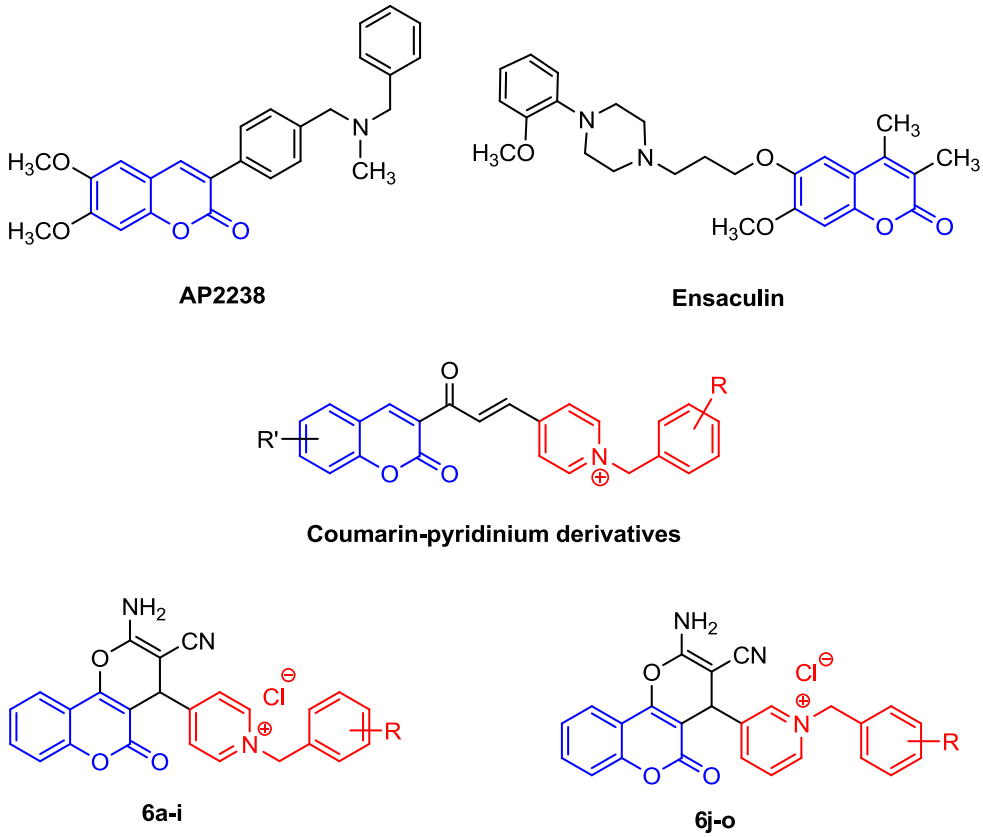

Fig. 2. Structures of coumarin containing AChE inhibitors, and designed fused coumarins **6a**–**o** as new inhibitors.

benzyl group of 4-pyridinium series improved anti-AChE potency as observed in compounds **6f**, **6h** and **6i**. The comparison of IC_{50} values of 2- or 3-chloro compounds **6b** and **6f** with their 2- or 3-fluoro analogs **6a** and **6d** revealed that the chlorine atom is more effective than fluorine in the *ortho* and *meta* positions.

In the 3-pyridinium series (compounds **6j**–**o**), the fluoro-substituted compounds **6j**, **6l** and **6o** showed approximately same inhibitory activity against AChE. This finding demonstrates that the regioisomerism of fluorine substituent on the *N*-benzyl group of 3-pyridinum series has no significant effect on inhibitory activity. In contrast, 2-chlorobenzyl derivative **6k** was significantly more active than 3-chlorobenzyl analog **6m**.

In the term of BuChE inhibitory activity in 4-pyridinium series, compounds **6g**–**i** containing halogen atom at *para*-position showed improved potency. By comparing the IC_{50} values of 2-chloro derivative **6b** with 2,4-dichloro analog **6i** or of 3-chloro derivative **6f** with corresponding 3,4-dichloro compound **6h**, it could be concluded that the introduction of second chlorine atom onto the

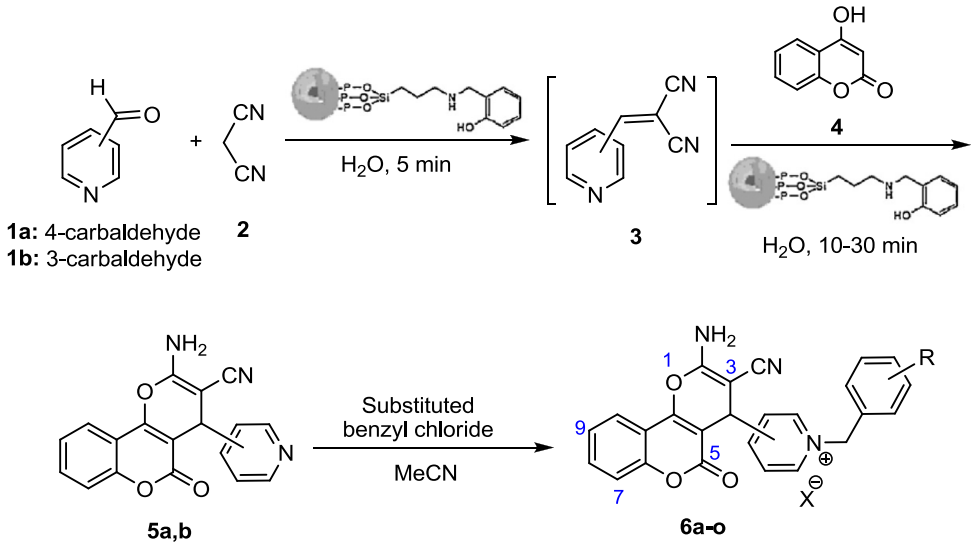

Scheme 1. Synthesis of 5-oxo-4,5-dihydropyrano[3,2-*c*]chromene derivatives.

Table 1
Inhibition of AChE from *Electrophorus electricus* (*eel*AChE) and horse serum butyrylcholinesterase (*eq*BuChE) by compounds **6a**–**o** in comparison with donepezil.

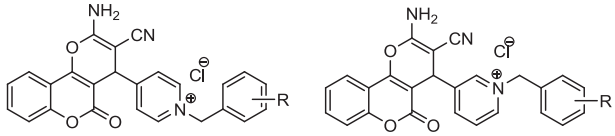

Compound	R	IC_{50} (μM)[a] *eel*AChE	IC_{50} (μM) *eq*BuChE	Selectivity[b]
6a	2-F	2.9 ± 0.17	36 ± 2.28	12.4
6b	2-Cl	1.5 ± 0.09	4.8 ± 0.3	3.2
6c	2-CH_3	3.7 ± 0.21	17.8 ± 1.13	4.8
6d	3-F	2.8 ± 0.16	>50	>17.8
6e	3-CH_3	1.9 ± 0.11	5.5 ± 0.35	2.6
6f	3-Cl	0.48 ± 0.03	21.8 ± 1.38	45.4
6g	4-F	0.038 ± 0.002	1.84 ± 0.12	48.4
6h	3,4-Cl_2	0.044 ± 0.002	1.27 ± 0.08	28.9
6i	2,4-Cl_2	0.831 ± 0.048	0.566 ± 0.004	0.68
6j	2-F	1.8 ± 0.1	41 ± 2.6	22.8
6k	2-Cl	1.0 ± 0.06	11.2 ± 0.71	11.2
6l	3-F	2.0 ± 0.12	>50	>25
6m	3-Cl	7.4 ± 0.43	38.4 ± 2.4	5.2
6n	3-CH_3	0.79 ± 0.04	14.3 ± 0.9	18.1
6o	4-F	2.17 ± 0.12	2.17 ± 0.14	1
Donepezil		0.014 ± 0.0008	5.38 ± 0.34	384.3

[a] Data are expressed as mean ± S.E. of at least three different experiments.
[b] Selectivity for AChE = IC_{50} (BuChE)/IC_{50} (AChE).

para-position of benzyl group increased the anti-BuChE activity. In addition, the translocation of fluorine atom on the *N*-benzyl-4-pyridinium moiety had significant effect on BuChE inhibitory activity, and *para*-fluoro was preferred. Replacement of fluorine atom at *ortho* or *meta* positions with chlorine atom increased BuChE-inhibition potency (compounds **6b** and **6f** vs. **6a** and **6d**, respectively).

The observed IC_{50} values of 3-pyridinium derivatives **6j**–**o** against BuChE revealed that the better result was obtained with 4-fluoro substituent (compound **6o**). Similar to the 4-pyridinium series, 2- or 3-chloro derivatives **6k** and **6m** were more active than 2- or 4-fluoro derivatives **6j** and **6l** against BuChE.

The comparison of IC_{50} values of 3-pyridinium derivatives with their corresponding 4-pyridinium regioisomers against AChE revealed that 3-pyridinium analogs **6j**–**l** and **6n** were more active than their regioisomers. In contrast, the anti-AChE activity of **6m** and **6o** was less than their 4-pyridinium regioisomers. In the 4-pyridinium series, 4-fluoro- and 3,4-dichloro derivatives were the most potent compounds, in the term of AChE inhibition. While amongst the 3-pyridinium derivatives, 3-methyl analog showed highest inhibitory activity against AChE. These results demonstrated that the effect of 3,4-regioisomerism of the pyridinium part depends on the type and the position of substituent on benzyl group.

It is worthy to note that in the cases of dichlorobenzyl derivatives **6h** and **6i**, regioisomerism of chlorine substitution could dramatically change the AChE/BuChE selectivity. While 2,4-dichlorobenzyl derivative **6i** has no significant selectivity, but 3,4-dichlorobenzyl counterpart **6h** shows relatively high selectivity for AChE.

Interestingly, both 4-fluorobenzyl analogs **6g** and **6o** have similar activity against BuChE, but the anti-AChE activity of 4-pyridinum derivative **6g** is about 57-fold more than that of 3-pyridinum congener **6o**.

In overall, the representative compound **6g** has a potent anti-AChE activity, which can inhibit AChE at the nano-molar concentrations with proper selectivity.

3.3. Docking studies

In order to explain the different activities of the target compounds and also to clarify their interaction mode in the active site of AChE, docking studies were conducted using Autodock Vina 1.1.1. Several Ligand-bounded crystallographic structures of AChE are available in the RCSB protein data bank (http://www.rcsb.org/pdb/home/home.do). In this study, the PDB structure of 3I6Z was retrieved for docking purposes. Since the AChE from *electrophorus electricus* was used for the experimental section and there were not any high resolution (<2.5 Å) crystallographic structures of this target in the PDB, therefore we used the high-resolution homologue structure (3I6Z: 2.19 Å) with 64% overall identity towards the native protein and 100% identity in the active site. The best pose of each ligand in terms of the free energy of binding was extracted from the 50 generated top scores. Since, compounds **6g** and **6n** were able to represent the whole chemical space and were more potent than their counterparts were subjected to further studies of binding mode. The best pose of the compounds in the gorge of AChE is depicted in Fig. 3.

As described, the chemical space is comprised of two fragments; a pyranochromen-2-one, and a *N*-benzylpyridinium part. A common feature of all compounds is their ability to interact with the two distinct regions in the active site, *viz* central anionic site (CAS) at the vicinity of the catalytic site (CS) and the peripheral anionic site (PAS) at the top the gorge of AChE. The most important residues responsible for the interaction of the synthesized inhibitors included Phe330, Trp84 in CAS and Trp279 in PAS, where Phe330 was the key residue in ligand recognition and trafficking. The aromatic part in pyranochromenone fragment was oriented so that a π–π interaction was possible with Phe330 and Trp84. In addition, the positively charged amino substituent on the pyran ring was prone to negative area caused by a carboxylic side chain of Asp72.

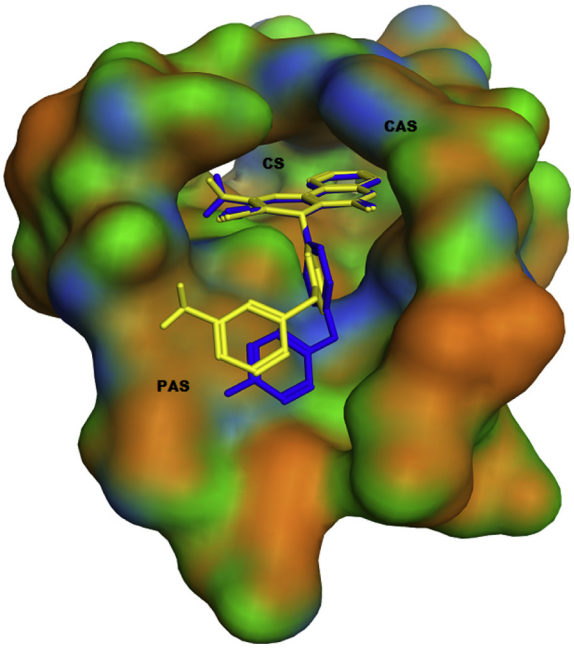

Fig. 3. The best pose of the compounds **6g** and **6n** obtained from docking study in the active site of AChE. The catalytic site (CS), central anionic site (CAS) and peripheral anionic site (PAS) were shown in the receptor. The blue and yellow colors were attributed to the **6g** and **6n** respectively. (For interpretation of the references to colour in this figure legend, the reader is referred to the web version of this article.)

In the compounds with enhanced activities (i.e. **6g**), an additional π–π interaction between the benzyl group on pyridinium ring and Trp279 led to stabilization of the resulting complex.

In the 4-pyridinium series, **6g** showed to be the most active compound and its binding mode in the active site is displayed in Fig. 4.

The presence of electron withdrawing groups such as fluoro or chloro on the proper position of the benzylic pendent could lead to reinforcing π–π interaction as in compounds **6g**, in comparison with **6c**. The order of activity is 4-F > 2-F ≈ 3-F for fluoro-substitution and 3-Cl > 2-Cl for chloro-substitution. This can be explained by the more feasible π–π interactions in the more potent compounds (Fig. 5).

As described above, when two chlorine atoms were attached to the benzyl moiety, the activity was largely dependent on their positions. The π–π interaction was destabilized in compound **6i** due to the disfavored orientation of lipophilic chlorine atom towards the hydrophilic pocket composed of ser286, Ile287 and Phe287, as depicted in Fig. 6.

In the case of compound **6e**, the presence of methyl at the 3-position of benzyl moiety led to unexpectedly increasing of the activity. This finding can be reasonably explained by π–H interaction between methyl hydrogens at position 3 and the phenyl ring of Tyr70 (Fig. 7). Among the 3-pyridinium derivatives, the most active compound was **6n** with a 3-methylbenzyl moiety. A π–H interaction similar to that observed for compound **6e** was responsible for its enhanced activity in comparison with compounds **6l** and **6m** containing 3-fluoro or 3-chlorobenzyl groups respectively (Fig. 8).

The most active compound against BuChE (compound **6i**) was used for docking with BuChE (PDB ID: 4BDS), and the best-docked pose was extracted for further study. The binding mode for the interaction of **6i** with the target structure is depicted in Fig. 9. The orientation of the ligand in the active site facilitated formation of a π–π stacking between coumarin ring and Trp79. Consequently, the partially charged amino and nitrile groups were exposed to oxyanionic hole composed by carbonyl moieties of Gln64, Asn65, Asp67, Asn80, Thr117 and Gly118. Moreover, the hydrophobic 2,4-dichlorophenyl moiety was well fitted in a hydrophobic pocket made by Pro282, Leu283, Phe326, Tyr329 and Gly330.

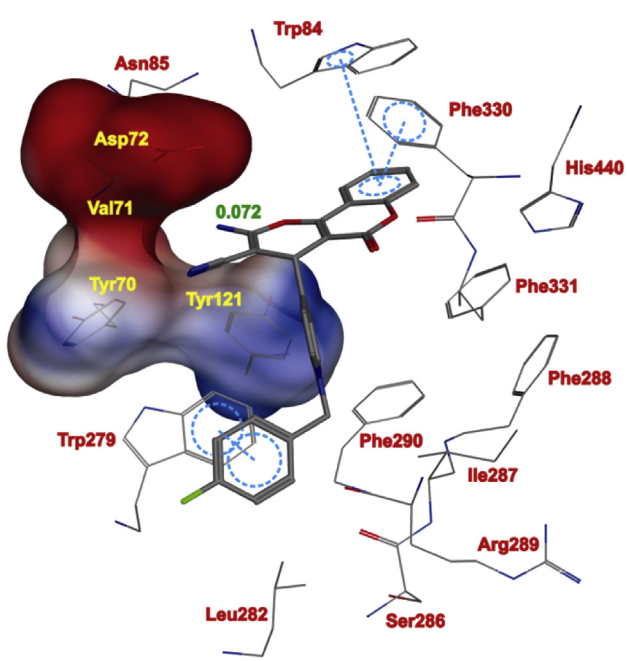

Fig. 4. A representative model for interaction of compound **6g** and the AChE. The π–π interaction is illustrated as a cyan dashed line. The calculated electrostatic potential map for Asp72, Val71, Tyr70 and Tyr121 is shown and partial charge for an amino group as well. (Red color: negatively charged region; Blue color: positively charged region). (For interpretation of the references to colour in this figure legend, the reader is referred to the web version of this article.)

3.4. ADMET prediction

The ADMET (Absorption, Distribution, Metabolism, Excretion and Toxicity) properties of the target compounds were calculated using some web-based applications. BBB (Blood-Brain Barrier) penetration, HIA (Human Intestinal Absorption), Caco-2 cell permeability and AMES test were calculated using admetSAR [19] a web-base application and LC_{50} values (Lethal concentration 50%) were predicted using http://lazar.in-silico.de/predict. The predicted ADMET data were summarized in Table 2. Based on the predicted values for BBB penetration, all compounds might be able to penetrate into the CNS and therefore, are considered as active compound on the CNS. Moreover, all the compounds may not show either acute toxicity according to the calculated LC50 values nor mutagenic effect with respect to the AMES test data. In addition, the Lipinski criteria for the target compounds were predicted and the data are provided in the Supplementary data. According to the Lipinski criteria of drug likeness, all compounds were within the range set by Lipinski's rule-of-five and could be good candidate for drug development.

3.5. Kinetic study of AChE inhibition

The mechanism of the enzyme inhibition was investigated using the most active compound **6g**. Three fixed concentrations of the inhibitor (2.1 nM, 21 nM and 105 nM) were chosen and for each concentration, the initial velocity (V) of the substrate hydrolysis was measured at different substrate (S) concentrations in the range of 0.14–0.69 mM. A plot of the reciprocal of the initial velocity (1/V) versus the reciprocal of the substrate concentration (1/S) was thereafter obtained. The Lineweaver–Burk plot showed increasing slopes and intercepts with higher inhibitor concentrations (Fig. 10). It was therefore concluded that a mixed-type inhibition could be attributed to the compound **6g**. The kinetic study was in agreement with the docking studies in which a dual binding site interaction with the receptor was observed.

4. Conclusion

In conclusion, we described a series of fused coumarins namely 5-oxo-4,5-dihydropyrano[3,2-*c*]chromenes linked to *N*-benzylpyridinium scaffold as new acetylcholinesterase inhibitors. Two distinct 3-pyridinium and 4-pyridinium derivatives were synthesized from appropriate pyridine-carbaldehyde, malononitrile and 4-hydroxycoumarin, and subsequent *N*-benzylation. The results of anti-cholinesterase activity toward AChE and BuChE revealed that the type and position of halogen on the benzyl pendent could regulate anti-AChE activity and AChE/BuChE selectivity. The 1-(4-fluorobenzyl) derivative **6g** from 4-pyridinium series showed the most potent anti-AChE activity (IC_{50} value = 0.038 μM) and the highest AChE/BuChE selectivity (SI > 48). Our docking study demonstrated the capability of prototype compounds to interact with the two distinct regions in the active site of AChE; the catalytic site and the peripheral anionic site. Moreover, the docking simulations permitted us to rationalize the observed structure–affinity relationships.

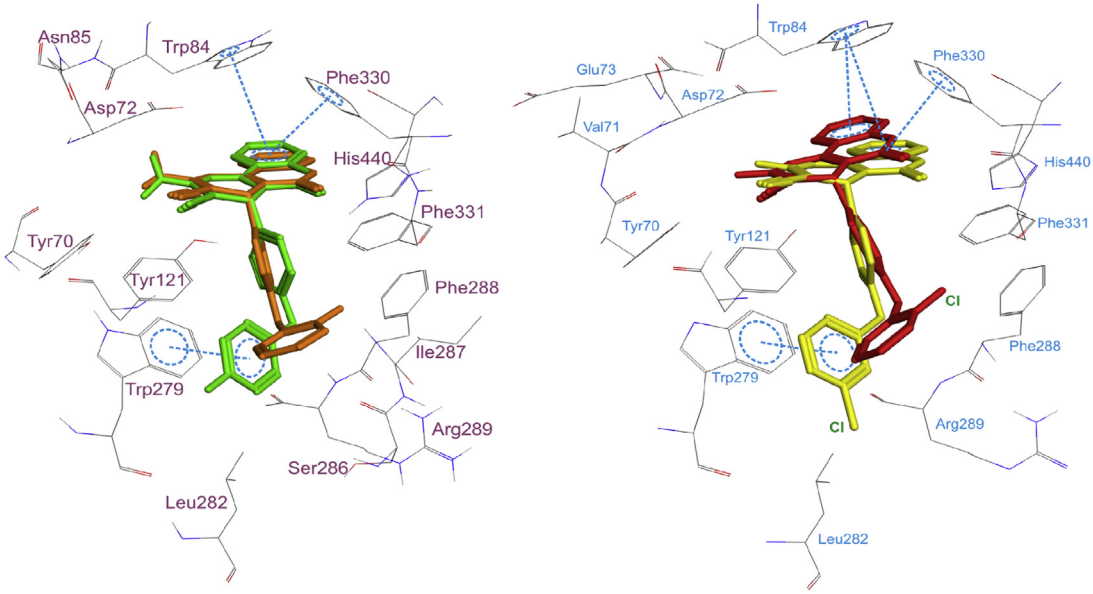

Fig. 5. The effect of halogen position on the orientation of phenyl ring toward Trp279. Left: 2-fluoro- and 4-fluoro derivatives (**6a** and **6g**) are shown in brown and green respectively. Right: 2-chloro and 3-chloro analogs (**6b** and **6f**) are illustrated in red and yellow, respectively. (For interpretation of the references to colour in this figure legend, the reader is referred to the web version of this article.)

5. Experimental

5.1. General methods

All commercially available reagents were used without further purification. The inorganic–organic hybrid magnetic nano-catalyst was synthesized following the protocol previously described by our group [18]. TLC was conducted on silica gel 250 micron, F254 plates. Melting points were measured with a Kofler hot stage apparatus and are uncorrected. The IR spectra were taken using Nicolet FT-IR Magna 550 spectrographs (KBr disks). ^{1}H NMR spectra were recorded on an NMR instrument Bruker 500 MHz. The chemical shifts (δ) and coupling constants (J) are expressed in parts per million and hertz, respectively. Mass spectra of the products were obtained with an HP (Agilent Technologies) 5937 Mass Selective Detector. Elemental analyses were carried out by a CHN-Rapid Heraeus elemental analyzer. The results of elemental analyses (C, H, N) were within ±0.4% of the calculated values.

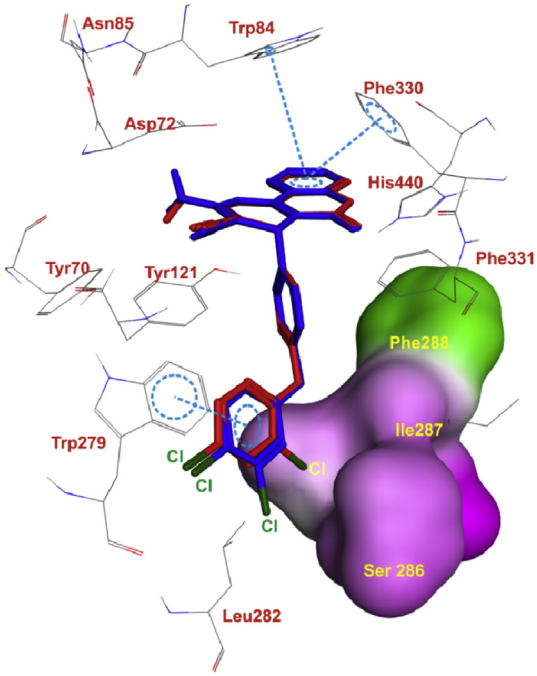

Fig. 6. Illustration of binding mode of **6h** (blue) and **6i** (red) in the active site of the enzyme. The calculated molecular surface for three amino acids in terms of their lipophilicity is shown. (The more hydrophilic surface is represented as pink). (For interpretation of the references to colour in this figure legend, the reader is referred to the web version of this article.)

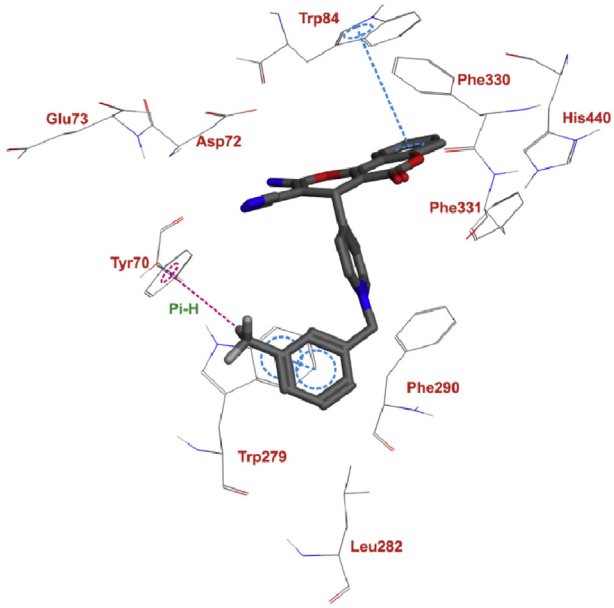

Fig. 7. Compound **6e** in the active site of the AChE enzyme. The probable Pi–H interaction of 3-methyl group with Tyr70 is shown by dashed line.

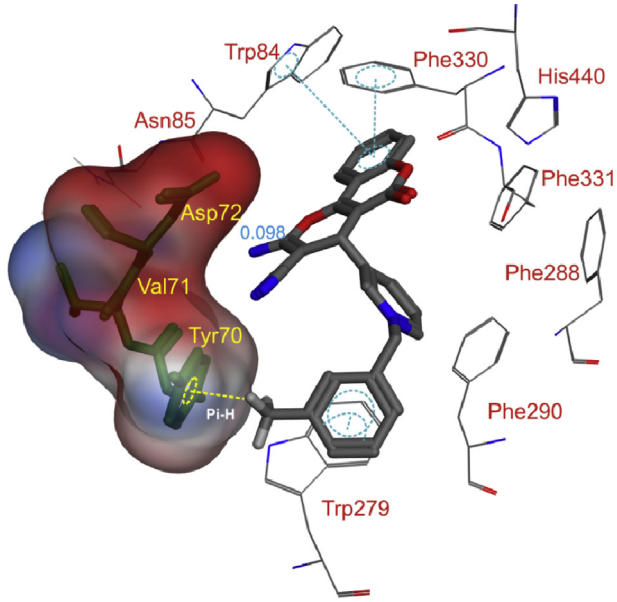

Fig. 8. An additional Pi–H interaction of compound **6n** with the Tyr70.

Table 2
Predicted ADMET properties of the target compounds **6a**–**o**.

Compound	R	BBB penetration		HIA[a] %	Caco-2 permeability[b]	AMES toxicity[c]	Acute toxicity LC_{50}[d] (μmol)
		%	CNS activity				
6a	2-F	0.84	+	0.98	–	–	2.85
6b	2-Cl	0.80	+	0.98	–	–	1.90
6c	2-CH_3	0.80	+	0.99	+	–	2.65
6d	3-F	0.84	+	0.98	–	–	2.85
6e	3-CH_3	0.80	+	0.99	+	–	2.65
6f	3-Cl	0.80	+	0.98	–	–	1.90
6g	4-F	0.84	+	0.98	–	–	2.85
6h	3,4-Cl_2	0.80	+	0.98	–	–	1.73
6i	2,4-Cl_2	0.80	+	0.98	–	–	1.73
6j	2-F	0.84	+	0.98	–	–	2.72
6k	2-Cl	0.80	+	0.98	–	–	1.81
6l	3-F	0.84	+	0.98	–	–	2.72
6m	3-Cl	0.80	+	0.98	–	–	1.81
6n	3-CH_3	0.80	+	0.99	+	–	2.54
6o	4-F	0.84	+	0.98	–	–	2.72
Donepezil	–	0.99	+	0.99	+	–	3

[a] Human intestinal absorption.
[b] The values more than **50** was considered as +.
[c] Mutagenic potential of chemicals.
[d] EPA v4b Fathead Minnow Acute Toxicity.

*5.2. General procedure for the synthesis of 2-amino-5-oxo-4-(pyridin-3 or 4-yl)-4,5-dihydropyrano[3,2-c]chromene-3-carbonitriles (**5a** or **5b**)*

A mixture of pyridine-carbaldehyde **1** (1 mmol), malononitrile (**2**, 1.2 mmol), magnetic catalytic system (1.5 mol%) and water (5 ml) was stirred at reflux for a few minutes. Then, 4-hydroxycoumarin (**4**, 1 mmol) was added. The mixture was refluxed for 30 min. After completion of the reaction which was monitored by TLC, it was allowed to cool at room temperature. The reaction mixture was diluted with ethyl acetate and the catalyst was easily separated with an external magnet and washed twice with ethyl acetate. The solvent was removed in vacuo, and the resultant solid was purified by recrystallization from ethanol.

*5.2.1. 2-Amino-5-oxo-4-(pyridin-4-yl)-4,5-dihydropyrano[3,2-c]chromene-3-carbonitrile (**5a**)*

Yield 70%; white solid; mp 270–272 °C [18]; IR (KBr, cm^{-1}) ν_{max}: 3354 and 3273 (NH_2), 2194 (CN), 1715 (C=O); ^1H NMR (500 MHz, DMSO-d_6) δ: 8.51 (d, 2H, $J = 4.5$ Hz, pyridine), 7.91 (d, 1H, $J = 7.5$ Hz, H_{10}), 7.72 (t, 1H, $J = 7.5$ Hz, H_8), 7.53 (s, 2H, NH_2), 7.51–7.45 (m, 2H, $H_{7,9}$), 7.33 (d, 2H, $J = 4.5$ Hz, pyridine), 4.51 (s, 1H, H_4). ^{13}C NMR (125 MHz, DMSO-d_6) δ: 159.5, 158.1, 154.0, 152.2, 151.7, 149.6, 133.1, 124.6, 122.9, 122.5, 118.8, 116.5, 112.8, 102.4, 56.4.

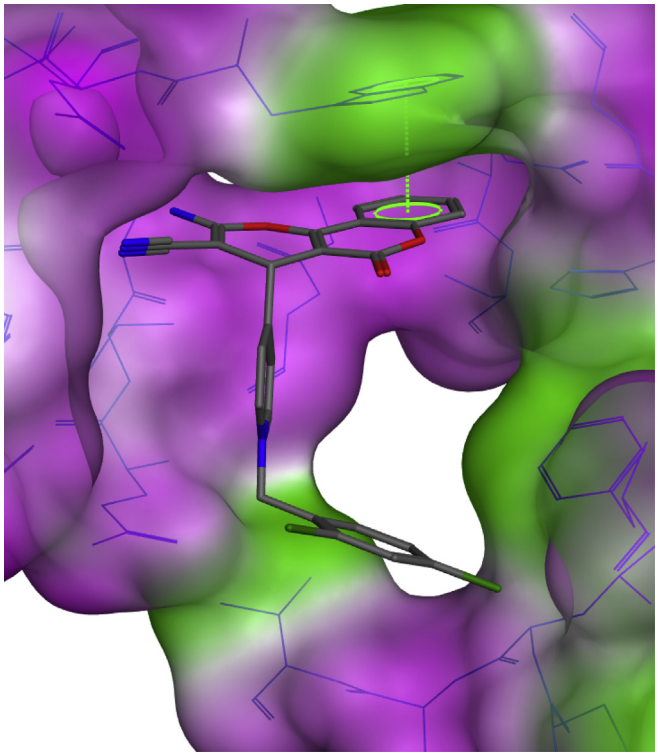

Fig. 9. The predicted binding mode of compound **6i** in the active site of BuChE.

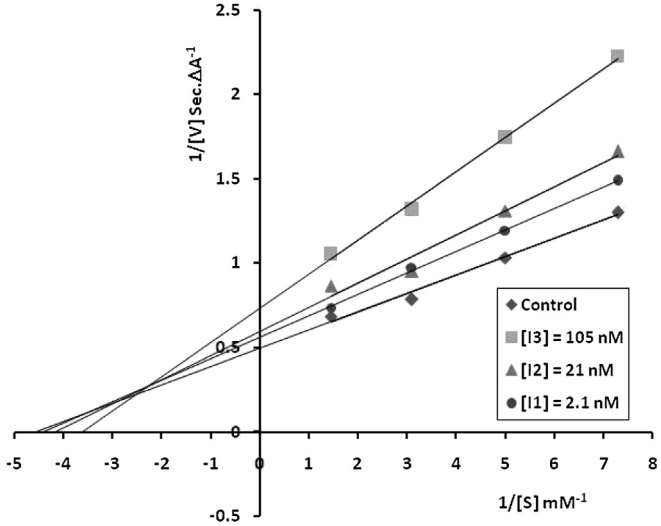

Fig. 10. The steady state inhibition of compound **6g**, against AChE. Reciprocal plot was based on the initial velocity and substrate concentration on increasing inhibitor concentrations. Lines were obtained from weighted least square analysis of the data points.

*5.2.2. 2-Amino-5-oxo-4-(pyridin-3-yl)-4,5-dihydropyrano[3,2-c] chromene-3-carbonitrile (**5b**)*

Yield 79%; white solid; mp 255–257 °C [18]; IR (KBr, cm^{-1}) ν_{max}: 3374 and 3284 (NH_2), 2193 (CN), 1708 (C=O); ^1H NMR (500 MHz, DMSO-d_6) δ: 8.85 (br s, 1H, pyridine), 8.46 (br s, 1H, pyridine), 7.89 (br s, 1H, pyridine), 7.70 (s, 2H, NH_2), 7.50–7.35 (m, 5H, H_{7-10} and pyridine), 4.55 (s, 1H, H_4). ^{13}C NMR (125 MHz, DMSO-d_6) δ: 159.5, 158.0, 153.7, 152.1, 149.0, 148.2, 138.7, 135.4, 132.9, 124.6, 123.7, 122.5, 119.0, 116.5, 112.8, 102.9, 56.9.

*5.3. General procedure for the synthesis of 3- or 4-(2-amino-3-cyano-5-oxo-4,5-dihydropyrano[3,2-c]chromen-4-yl)-1-(benzyl) pyridinium chloride derivatives **6a–o***

Compound **5** (1 mmol), appropriate benzyl chloride (1.2 mmol) and a catalytic amount of KI in dry acetonitrile (5 ml) was refluxed for 10–16 h. When the reaction was completed as indicated by TLC, the mixture was then concentrated under reduced pressure, and 5 ml of diethyl ether was added. The products **6a–o** were collected by filtration in good yields.

*5.3.1. 4-(2-Amino-3-cyano-5-oxo-4,5-dihydropyrano[3,2-c] chromen-4-yl)-1-(2-fluorobenzyl)pyridinium chloride (**6a**)*

Yield 90%; yellow solid; mp 191–194 °C; IR (KBr, cm^{-1}) ν_{max}: 3423 and 3321 (NH_2), 2189 (CN), 1718 (C=O); ^1H NMR (500 MHz, DMSO-d_6) δ: 9.12 (d, 2H, pyridine, $J = 5.9$ Hz), 8.23 (d, 2H, pyridine, $J = 5.9$ Hz), 7.94 (d, 1H, H_{10}, $J = 7.5$ Hz), 7.85 (s, 2H, NH_2), 7.76 (t, 1H, H_8, $J = 7.5$ Hz), 7.63 (t, 1H, phenyl, $J = 7.1$ Hz), 7.55–7.43 (m, 3H, $H_{7,9}$ and phenyl), 7.33–7.29 (m, 2H, phenyl), 5.95 (s, 2H, CH_2), 4.93 (s, 1H, H_4). ^{13}C NMR (125 MHz, DMSO-d_6) δ: 162.0, 161.5, 159.8, 159.6, 158.4, 154.9, 152.4, 145.1, 133.5, 132.2, 131.6, 127.4, 125.3, 124.9, 122.8, 121.2, 118.5, 116.7, 116.2, 116.0, 112.9, 100.8, 57.4, 54.5. EI-MS (m/z, %) 426 (M^+, 2), 313 (61), 121 (85), 109 (100), 83 (70). Anal. Calcd for $C_{25}H_{17}ClFN_3O_3$: C, 65.01; H, 3.71; N, 9.10. Found: C, 65.35; H, 3.54; N, 8.92.

*5.3.2. 4-(2-Amino-3-cyano-5-oxo-4,5-dihydropyrano[3,2-c] chromen-4-yl)-1-(2-chlorobenzyl)pyridinium chloride (**6b**)*

Yield 75%; orange solid; mp 146–149 °C; IR (KBr, cm^{-1}) ν_{max}: 3451 and 3385 (NH_2), 2193 (CN), 1717 (C=O); ^1H NMR (500 MHz, DMSO-d_6) δ: 9.06 (d, 2H, pyridine, $J = 5.9$ Hz), 8.23 (d, 2H, pyridine, $J = 5.9$ Hz), 7.92 (d, 1H, H_{10}, $J = 7.5$ Hz), 7.82 (s, 2H, NH_2), 7.77 (t, 1H, H_8, $J = 7.5$ Hz), 7.61–7.48 (m, 6H, $H_{7,9}$ and phenyl), 5.97 (s, 2H, CH_2), 4.96 (s, 1H, H_4). ^{13}C NMR (125 MHz, DMSO-d_6) δ: 162.4, 161.1, 155.0, 153.1, 144.9, 144.0, 133.2, 131.9, 131.7, 131.4, 131.2, 130.1, 128.1, 127.8, 125.9, 125.3, 122.6, 121.7, 119.4, 115.8, 65.6, 60.4. Anal. Calcd for $C_{25}H_{17}Cl_2N_3O_3$: C, 62.77; H, 3.58; N, 8.78. Found: C, 62.54; H, 3.44; N, 9.06.

*5.3.3. 4-(2-Amino-3-cyano-5-oxo-4,5-dihydropyrano[3,2-c] chromen-4-yl)-1-(2-methylbenzyl)pyridinium chloride (**6c**)*

Yield 91%; yellow solid; mp 233–236 °C; IR (KBr, cm^{-1}) ν_{max}: 3427 and 3239 (NH_2), 2189 (CN), 1727 (C=O); ^1H NMR (500 MHz, DMSO-d_6) δ: 9.05 (d, 2H, pyridine, $J = 6.5$ Hz), 8.23 (d, 2H, pyridine, $J = 6.5$ Hz), 7.97 (d, 1H, H_{10}, $J = 7.5$ Hz), 7.88 (s, 2H, NH_2), 7.77 (t, 1H, H_8, $J = 7.5$ Hz), 7.54–7.48 (m, 2H, $H_{7,9}$), 7.36–7.27 (m, 3H, phenyl), 7.17 (d, 1H, phenyl, $J = 7.4$ Hz), 5.94 (s, 2H, CH_2), 4.94 (s, 1H, H_4), 2.26 (s, 3H, CH_3). ^{13}C NMR (125 MHz, DMSO-d_6) δ: 161.8, 159.7, 158.4, 154.8, 152.4, 145.0, 136.9, 133.4, 132.2, 130.9, 129.4, 129.2, 127.2, 126.6, 124.8, 122.8, 118.4, 116.6, 112.8, 100.7, 60.9, 54.4, 18.7. Anal. Calcd for $C_{26}H_{20}ClN_3O_3$: C, 68.20; H, 4.40; N, 9.18. Found: C, 67.92; H, 4.11; N, 9.32.

*5.3.4. 4-(2-Amino-3-cyano-5-oxo-4,5-dihydropyrano[3,2-c] chromen-4-yl)-1-(3-fluorobenzyl)pyridinium chloride (**6d**)*

Yield 93%; yellow solid; mp 247–250 °C; IR (KBr, cm^{-1}) ν_{max}: 3469 and 3395 (NH_2), 2193 (CN), 1719 (C=O); ^1H NMR (500 MHz, DMSO-d_6) δ: 9.25 (d, 2H, pyridine, $J = 5.8$ Hz), 8.23 (d, 2H, pyridine, $J = 5.8$ Hz), 7.95 (d, 1H, H_{10}, $J = 7.6$ Hz), 7.84 (s, 2H, NH_2), 7.76 (t, 1H, H_8, $J = 7.6$ Hz), 7.55–7.37 (m, 5H, $H_{7,9}$ and phenyl), 7.32–7.25 (m, 1H, phenyl), 5.87 (s, 2H, CH_2), 4.92 (s, 1H, H_4). ^{13}C NMR (125 MHz, DMSO-d_6) δ: 161.8, 159.7, 158.4, 154.9, 152.4, 144.9, 133.4, 131.4, 127.3, 125.1, 124.8, 122.8, 118.4, 116.6, 116.4, 116.2, 116.1, 115.9, 112.9, 100.7, 61.8, 54.4. Anal. Calcd for $C_{25}H_{17}ClFN_3O_3$: C, 65.01; H, 3.71; N, 9.10. Found: C, 65.28; H, 3.64; N, 9.29.

*5.3.5. 4-(2-Amino-3-cyano-5-oxo-4,5-dihydropyrano[3,2-c] chromen-4-yl)-1-(3-methylbenzyl)pyridinium chloride (**6e**)*

Yield 92%; yellow solid; mp 244–247 °C; IR (KBr, cm^{-1}) ν_{max}: 3472 and 3243 (NH_2), 2194 (CN), 1722 (C=O); ^1H NMR (500 MHz, DMSO-d_6) δ: 9.22 (d, 2H, pyridine, $J = 6.5$ Hz), 8.22 (d, 2H, pyridine, $J = 6.5$ Hz), 7.95 (d, 1H, H_{10}, $J = 7.8$ Hz), 7.85 (s, 2H, NH_2), 7.76 (t, 1H, H_8, $J = 7.8$ Hz), 7.52 (t, 1H, H_9, $J = 7.8$ Hz), 7.48 (d, 1H, H_7, $J = 7.8$ Hz), 7.40 (s, 1H, phenyl), 7.37 (d, 1H, phenyl, $J = 7.5$ Hz), 7.32 (t, 1H, phenyl, $J = 7.5$ Hz), 7.23 (d, 1H, phenyl, $J = 7.5$ Hz), 5.84 (s, 2H, CH_2), 4.91 (s, 1H, H_4), 2.30 (s, 3H, CH_3). ^{13}C NMR (125 MHz, DMSO-d_6) δ: 161.6, 159.7, 158.3, 155.8, 154.9, 152.3, 144.8, 138.6, 134.1, 133.4, 130.0, 129.4, 129.1, 127.3, 125.9, 124.8, 122.8, 118.4, 116.6, 112.8, 100.7, 62.6, 54.4, 20.8. EI-MS (m/z, %) 422 (M^+, 3), 239 (36), 162 (38), 121 (63), 105 (100), 91 (73), 77 (67). Anal. Calcd for $C_{26}H_{20}ClN_3O_3$: C, 68.20; H, 4.40; N, 9.18. Found: C, 68.42; H, 4.14; N, 9.02.

*5.3.6. 4-(2-Amino-3-cyano-5-oxo-4,5-dihydropyrano[3,2-c] chromen-4-yl)-1-(3-chlorobenzyl)pyridinium chloride (**6f**)*

Yield 90%; yellow solid; mp 240–242 °C; IR (KBr, cm^{-1}) ν_{max}: 3465 and 3395 (NH_2), 2193 (CN), 1718 (C=O); ^1H NMR (500 MHz, DMSO-d_6) δ: 9.22 (d, 2H, pyridine, $J = 5.9$ Hz), 8.22 (d, 2H, pyridine, $J = 5.9$ Hz), 7.94 (d, 1H, H_{10}, $J = 7.5$ Hz), 7.83 (s, 2H, NH_2), 7.76–7.74 (m, 2H, H_8 and phenyl), 7.55–7.48 (m, 5H, $H_{7,9}$ and phenyl), 5.83 (s, 2H, CH_2), 4.92 (s, 1H, H_4). ^{13}C NMR (125 MHz, DMSO-d_6) δ: 161.8, 159.7, 158.3, 154.9, 152.3, 144.9, 136.3, 133.6, 133.4, 131.1, 129.4, 129.0, 127.7, 127.4, 124.8, 122.7, 118.4, 116.6, 112.8, 100.7, 61.8, 54.4, 36.5. EI-MS (m/z, %) 442 (M^+, 2), 223 (100), 150 (95), 127 (24), 125 (63), 91 (91), 57 (92), 43 (74). Anal. Calcd for $C_{25}H_{17}Cl_2N_3O_3$: C, 62.77; H, 3.58; N, 8.78. Found: C, 63.05; H, 3.74; N, 8.92.

*5.3.7. 4-(2-Amino-3-cyano-5-oxo-4,5-dihydropyrano[3,2-c] chromen-4-yl)-1-(4-fluorobenzyl)pyridinium chloride (**6g**)*

Yield 89%; yellow solid; mp > 250 °C; IR (KBr, cm^{-1}) ν_{max}: 3478 and 3395 (NH_2), 2194 (CN), 1713 (C=O); ^1H NMR (500 MHz, DMSO-d_6) δ: 9.23 (d, 2H, pyridine, $J = 5.9$ Hz), 8.23 (d, 2H, pyridine, $J = 5.9$ Hz), 7.95 (d, 1H, H_{10}, $J = 7.5$ Hz), 7.85 (s, 2H, NH_2), 7.78–7.70 (m, 3H, H_8, 2H phenyl), 7.54–7.47 (m, 2H, $H_{7,9}$), 7.37–7.27 (m, 2H, phenyl), 5.84 (s, 2H, CH_2), 4.92 (s, 1H, H_4). Anal. Calcd for $C_{25}H_{17}ClFN_3O_3$: C, 65.01; H, 3.71; N, 9.10. Found: C, 65.20; H, 3.63; N, 9.38.

*5.3.8. 4-(2-Amino-3-cyano-5-oxo-4,5-dihydropyrano[3,2-c] chromen-4-yl)-1-(3,4-dichlorobenzyl)pyridinium chloride (**6h**)*

Yield 70%; orange solid; mp > 250 °C; IR (KBr, cm^{-1}) ν_{max}: 3431 and 3375 (NH_2), 2193 (CN), 1717 (C=O); ^1H NMR (500 MHz, DMSO-d_6) δ: 9.26 (d, 2H, pyridine, $J = 5.9$ Hz), 8.22 (d, 2H, pyridine, $J = 5.9$ Hz), 8.02 (s, 1H, phenyl), 7.95 (d, 1H, H_{10}, $J = 7.5$ Hz), 7.86 (s, 2H, NH_2), 7.74 (t, 1H, H_8, $J = 7.5$ Hz), 7.64 (d, 1H, phenyl, $J = 7.5$ Hz), 7.53–7.49 (m, 4H, $H_{7,9}$ and phenyl), 5.87 (s, 2H, CH_2), 4.92 (s, 1H, H_4). Anal. Calcd for $C_{25}H_{16}Cl_3N_3O_3$: C, 58.56; H, 3.15; N, 8.19. Found: C, 58.35; H, 3.27; N, 8.34.

*5.3.9. 4-(2-Amino-3-cyano-5-oxo-4,5-dihydropyrano[3,2-c] chromen-4-yl)-1-(2,4-dichlorobenzyl)pyridinium chloride (**6i**)*

Yield 77%; orange solid; mp > 250 °C; IR (KBr, cm^{-1}) ν_{max}: 3451 and 3385 (NH_2), 2193 (CN), 1717 (C=O); ^1H NMR (500 MHz,

DMSO-d_6) δ: 9.06 (d, 2H, pyridine, J = 5.9 Hz), 8.23 (d, 2H, pyridine, J = 5.9 Hz), 7.94 (d, 1H, H_{10}, J = 7.5 Hz), 7.87 (s, 2H, NH_2), 7.85–7.77 (m, 2H, H_8 and phenyl), 7.66–7.49 (m, 4H, $H_{7,9}$ and phenyl), 5.98 (s, 2H, CH_2), 4.96 (s, 1H, H_4). Anal. Calcd for $C_{25}H_{16}Cl_3N_3O_3$: C, 58.56; H, 3.15; N, 8.19. Found: C, 58.35; H, 3.27; N, 8.34.

5.3.10. 3-(2-Amino-3-cyano-5-oxo-4,5-dihydropyrano[3,2-c] chromen-4-yl)-1-(2-fluorobenzyl)pyridinium chloride (**6j**)

Yield 92%; green solid; mp 222–225 °C; IR (KBr, cm^{-1}) ν_{max}: 3433 and 3388 (NH_2), 2190 (CN), 1708 (C=O); ^{1}H NMR (500 MHz, DMSO-d_6) δ: 9.37 (s, 1H, pyridine), 9.03 (d, 1H, pyridine, J = 5.8 Hz), 8.73 (d, 1H, pyridine, J = 6.8 Hz), 8.17–8.15 (m, 1H, pyridine), 7.96 (d, 1H, H_{10}, J = 7.6 Hz), 7.81–7.76 (m, 3H, NH_2 and H_8), 7.55–7.40 (m, 4H, $H_{7,9}$ and phenyl), 7.45–7.21 (m, 2H, phenyl), 5.98 (s, 2H, CH_2), 4.92 (s, 1H, H_4). ^{13}C NMR (125 MHz, DMSO-d_6) δ: 159.7, 158.3, 154.5, 152.3, 145.6, 144.7, 144.0, 143.8, 133.3, 131.9, 130.8, 128.2, 125.1, 124.7, 122.8, 118.5, 116.6, 116.0, 115.8, 112.8, 100.9, 57.9, 54.9. Anal. Calcd for $C_{25}H_{17}ClFN_3O_3$: C, 65.01; H, 3.71; N, 9.10. Found: C, 65.28; H, 3.56; N, 8.89.

5.3.11. 3-(2-Amino-3-cyano-5-oxo-4,5-dihydropyrano[3,2-c] chromen-4-yl)-1-(2-chlorobenzyl)pyridinium chloride (**6k**)

Yield 87%; green solid; mp 222–225 °C; IR (KBr, cm^{-1}) ν_{max}: 3458 and 3385 (NH_2), 2189 (CN), 1709 (C=O); ^{1}H NMR (500 MHz, DMSO-d_6) δ: 9.41 (s, 1H, pyridine), 8.94 (d, 1H, pyridine, J = 6.1 Hz), 8.76 (d, 1H, pyridine, J = 7.7 Hz), 8.17–8.15 (m, 1H, pyridine), 7.97 (d, 1H, H_{10}, J = 7.4 Hz), 7.82 (s, 2H, NH_2), 7.76 (t, 1H, H_8, J = 7.4 Hz), 7.60–7.42 (m, 5H, $H_{7,9}$ and phenyl), 7.32 (d, 1H, phenyl, J = 7.4 Hz), 6.01 (s, 2H, CH_2), 4.93 (s, 1H, H_4). ^{13}C NMR (125 MHz, DMSO-d_6) δ: 159.7, 158.3, 154.5, 152.3, 145.6, 145.3, 143.9, 143.8, 133.4, 133.0, 131.6, 131.2, 130.8, 130.0, 128.2, 128.0, 124.8, 122.8, 118.6, 116.6, 112.8, 100.9, 61.3, 55.0. Anal. Calcd for $C_{25}H_{17}Cl_2N_3O_3$: C, 62.77; H, 3.58; N, 8.78. Found: C, 62.41; H, 3.75; N, 8.73.

5.3.12. 3-(2-Amino-3-cyano-5-oxo-4,5-dihydropyrano[3,2-c] chromen-4-yl)-1-(3-fluorobenzyl)pyridinium chloride (**6l**)

Yield 89%; yellow solid; mp 188–190 °C; IR (KBr, cm^{-1}) ν_{max}: 3442 and 3395 (NH_2), 2194 (CN), 1713 (C=O); ^{1}H NMR (500 MHz, DMSO-d_6) δ: 9.46 (s, 1H, pyridine), 9.13 (d, 1H, pyridine, J = 6.1 Hz), 8.73 (d, 1H, pyridine, J = 8.0 Hz), 8.17–8.15 (m, 1H, pyridine), 7.94 (dd, 1H, H_{10}, J = 7.9 and 1.5 Hz), 7.79 (s, 2H, NH_2), 7.76 (dt, 1H, H_8, J = 7.9 and 1.5 Hz), 7.55–7.45 (m, 3H, $H_{7,9}$ and phenyl), 7.39–7.35 (m, 1H, phenyl), 7.31 (d, 1H, phenyl, J = 7.7 Hz), 7.28–7.24 (m, 1H, phenyl), 5.87 (s, 2H, CH_2), 4.90 (s, 1H, H_4). ^{13}C NMR (125 MHz, DMSO-d_6) δ: 163.1, 161.1, 159.8, 158.4, 154.6, 152.4, 145.5, 144.4, 144.1, 143.8, 136.7, 133.4, 131.2, 128.4, 124.8, 124.5, 122.8, 118.7, 116.6, 116.3, 115.5, 115.4, 112.9, 100.9, 62.4, 55.0. Anal. Calcd for $C_{25}H_{17}ClFN_3O_3$: C, 65.01; H, 3.71; N, 9.10. Found: C, 65.24; H, 3.58; N, 9.33.

5.3.13. 3-(2-Amino-3-cyano-5-oxo-4,5-dihydropyrano[3,2-c] chromen-4-yl)-1-(3-chlorobenzyl)pyridinium chloride (**6m**)

Yield 90%; yellow solid; mp 217–221 °C; IR (KBr, cm^{-1}) ν_{max}: 3467 and 3398 (NH_2), 2193 (CN), 1715 (C=O); ^{1}H NMR (500 MHz, DMSO-d_6) δ: 9.48 (s, 1H, pyridine), 9.17 (d, 1H, pyridine, J = 6.1 Hz), 8.72 (d, 1H, pyridine, J = 7.7 Hz), 8.17–8.15 (m, 1H, pyridine), 7.97 (d, 1H, H_{10}, J = 7.7 Hz), 7.81 (s, 2H, NH_2), 7.76 (t, 1H, H_8, J = 7.7 Hz), 7.63 (s, 1H, phenyl), 7.54–7.44 (m, 5H, phenyl and $H_{7,9}$), 5.88 (s, 2H), 4.90 (s, 1H, H_4). ^{13}C NMR (125 MHz, DMSO-d_6) δ: 159.7, 158.3, 154.5, 152.3, 145.4, 144.4, 144.1, 143.7, 136.5, 133.6, 133.4, 131.0, 129.2, 128.4, 127.1, 124.7, 122.8, 118.6, 116.6, 112.8, 100.9, 62.3, 54.9. Anal. Calcd for $C_{25}H_{17}Cl_2N_3O_3$: C, 62.77; H, 3.58; N, 8.78. Found: C, 62.93; H, 3.44; N, 8.86.

5.3.14. 3-(2-Amino-3-cyano-5-oxo-4,5-dihydropyrano[3,2-c] chromen-4-yl)-1-(3-methylbenzyl)pyridinium chloride (**6n**)

Yield 90%; yellow solid; mp 195–198 °C; IR (KBr, cm^{-1}) ν_{max}: 3426 and 3343 (NH_2), 2202 (CN), 1719 (C=O); ^{1}H NMR (500 MHz, DMSO-d_6) δ: 9.47 (s, 1H, pyridine), 9.10 (d, 1H, pyridine, J = 6.1 Hz), 8.71 (d, 1H, pyridine, J = 7.5 Hz), 8.18–8.16 (m, 1H, pyridine), 7.96 (d, 1H, H_{10}, J = 7.6 Hz), 7.81–7.76 (m, 3H, NH_2 and H_8), 7.55–7.48 (m, 2H, $H_{7,9}$), 7.35–7.21 (m, 5H, phenyl), 5.83 (s, 2H, CH_2), 4.91 (s, 1H, H_4), 2.27 (s, 3H, Me). ^{13}C NMR (125 MHz, DMSO-d_6) δ: 159.7, 158.3, 154.6, 152.4, 145.2, 144.3, 144.1, 143.6, 138.5, 134.3, 133.4, 129.7, 129.0, 128.6, 128.3, 125.2, 124.8, 122.7, 118.6, 116.6, 112.9, 100.9, 63.2, 55.0, 20.8. Anal. Calcd for $C_{26}H_{20}ClN_3O_3$: C, 68.20; H, 4.40; N, 9.18. Found: C, 68.33; H, 4.24; N, 9.03.

5.3.15. 3-(2-Amino-3-cyano-5-oxo-4,5-dihydropyrano[3,2-c] chromen-4-yl)-1-(4-fluorobenzyl)pyridinium chloride (**6o**)

Yield 74%; yellow solid; mp > 250 °C; IR (KBr, cm^{-1}) ν_{max}: 3428 and 3379 (NH_2), 2194 (CN), 1713 (C=O); ^{1}H NMR (500 MHz, DMSO-d_6) δ: 9.45 (s, 1H, pyridine), 9.13 (d, 1H, pyridine, J = 5.3 Hz), 8.71 (d, 1H, pyridine, J = 7.5 Hz), 8.16–8.14 (m, 1H, pyridine), 7.96 (d, 1H, H_{10}, J = 7.4 Hz), 7.80–7.75 (m, 3H, H_8 and NH_2), 7.59–7.47 (m, 4H, $H_{7,9}$ and phenyl), 7.30–7.26 (m, 2H, phenyl), 5.86 (s, 2H, CH_2), 4.90 (s, 1H, H_4). ^{13}C NMR (125 MHz, DMSO-d_6) δ: 163.4, 161.5, 159.7, 158.3, 154.5, 152.4, 145.3, 144.2, 144.0, 143.5, 133.4, 131.0, 130.5, 128.3, 124.8, 122.7, 118.6, 116.6, 116.1, 115.9, 112.9, 100.9, 62.4, 55.0. Anal. Calcd for $C_{25}H_{17}ClFN_3O_3$: C, 65.01; H, 3.71; N, 9.10. Found: C, 65.20; H, 3.63; N, 9.38.

5.4. Pharmacology

The inhibitory potency of target compounds on AChE and BuChE was determined using Ellman's method [20]. Acetylcholinesterase (AChE, E.C. 3.1.1.7, Type V–S, lyophilized powder, from *electric eel,* 1000 units), butyrylcholinesterase (BuChE, E.C. 3.1.1.8, from equine serum) and butyrylthiocholine iodide were obtained from Sigma–Aldrich. 5,5′-Dithiobis-(2-nitrobenzoic acid) (DTNB), potassium dihydrogen phosphate, dipotassium hydrogen phosphate, potassium hydroxide, sodium hydrogen carbonate, and acetylthiocholine iodide were purchased from Fluka. The stock solutions of testing compounds were prepared by dissolving them in DMSO (1 ml) and phosphate buffer (9 ml). Five concentrations of the testing compounds in the range from 10^{-3} to 10^{-7} M were tested. The reaction mixture included 100 μl of DTNB 0.1 M, 50 μl of enzyme (2 U/ml), 50 μl of inhibitor solution and 10 μl of substrate (acetylthiocholine iodide or butyrylthiocholine iodide) 0.15 M. The changing of the absorbance was measured at 412 nm for 2 min. The IC_{50} values were determined graphically from inhibition curves (log inhibitor concentration vs. percent of inhibition). A UV-2100 Rayleigh Double Beam Spectrophotometer was used for spectrophotometric measurements.

5.5. Molecular docking study

The pdb structure of 3I6Z was retrieved for docking purposes as a complex co-crystallized with inhibitor *N*-sacharinohexyl-galantamine. Then, the amino acid chain was kept and the water molecules and co-crystallized ligand were removed and subsequently the missing atom types were repaired using Modeller 9.11. Afterward, the polar hydrogen was added to the receptor and the resulting protein was subjected to minimization using OPLS2005 force field. The prepared protein was saved in pdbqt format using Autodock Tools 1.5.4 [21]. The ligand coordinates were generated using MarvineSketch 5.8.3, 2012, ChemAxon (http://www.chemaxon.com), which was converted to 3D structure using Openbabel version (2.3.1) [22]. Finally the pdbqt formats (The input

format of docking software) of the ligands were prepared with Autodock Tools 1.5.4 using default parameters. Autodock Vina (ver. 1.1.1) [23] was used for docking calculations with default parameters except for exhaustiveness that was set to 80. For all the docking calculations, a grid box size of 40 × 40 × 40, centered at the geometrical center of co-crystallized ligand was used. The coordinates *x*, *y*, *z* for the center of grid box were 3.755, 63.699, 65.983, respectively. To validate our docking procedure, the co-crystallized ligand was re-docked into the active site of the enzyme and the reasonable RMSD value of 1.947 Å was obtained. Finally, the conformations with the most favorable free energy of binding were selected for analyzing the interactions between the AChE and inhibitor. All the 3D models are generated using the Chimera 1.6 software [24]. The same procedure was applied in the case of BuChE.

Acknowledgments

This work was supported by grants from the Research Council of Tehran University of Medical Sciences, Iran National Elite Foundation (INEF) and the Iran National Science Foundation (INSF). Molecular graphics and analyses were performed with the UCSF Chimera package. Chimera is developed by the 25 Resource for Biocomputing, Visualization, and Informatics at the University of California, San Francisco.

Appendix A. Supplementary data

Supplementary data related to this article can be found at http://dx.doi.org/10.1016/j.ejmech.2013.07.038.

References

[1] A.V. Terry Jr., J.J. Buccafusco, The cholinergic hypothesis of age and Alzheimer's disease-related cognitive deficits: recent challenges and their implications for novel drug development, J. Pharmacol. Exp. Ther. 306 (2003) 821–827.
[2] M.G. Cardozo, T. Kawai, Y. Iimura, H. Sugimoto, Y. Yamanishi, A.J. Hopfinger, Conformational analyses and molecular-shape comparisons of a series of indanone-benzylpiperidine inhibitors of acetylcholinesterase, J. Med. Chem. 35 (1992) 590–601.
[3] M.R. Roberson, L.E. Harrell, Cholinergic activity and amyloid precursor protein metabolism, Brain Res. Brain Res. Rev. 25 (1997) 50–69.
[4] R.E. Fine, The biochemistry of Alzheimer disease, Alzheimer Dis. Assoc. Disord. 13 (Suppl. 1) (1999) S82–S87.
[5] J.L. Cummings, Alzheimer's disease, N. Engl. J. Med. 351 (2004) 56–67.
[6] (a) E. Giacobini, Cholinesterase inhibitors: new roles and therapeutic alternatives, Pharmacol. Res. 50 (2004) 433–440;
(b) M.A. Kamal, P. Klein, W. Luo, Y. Li, H.W. Holloway, D. Tweedie, et al., Kinetics of human serum butyrylcholinesterase inhibition by a novel experimental Alzheimer therapeutic dihydrobenzodioxepine cymserine, Neurochem. Res. 33 (2008) 745–753;
(c) R.M. Lane, S.G. Potkin, A. Enz, Targeting acetylcholinesterase and butyrylcholinesterase in dementia, Int. J. Neuropsychopharmacol. 9 (2005) 1–24.
[7] G.G. Osborn, A.V. Saunders, Current treatments for patients with Alzheimer disease, J. Am. Osteopath. Assoc. 110 (2010) S16–S26.
[8] E.G. McGeer, P.L. McGeer, Clinically tested drugs for Alzheimer's disease, Expert Opin. Investig. Drugs 12 (2003) 1143–1151.
[9] A. Castro, A. Martinez, Peripheral and dual binding site acetylcholinesterase inhibitors: implications in treatment of Alzheimer's disease, Mini Rev. Med. Chem. 1 (2001) 267–272.
[10] E. Giacobini, Cholinesterases: new roles in brain function and in Alzheimer's disease, Neurochem. Res. 28 (2003) 515–522.
[11] M. Pera, A. Martinez-Otero, L. Colombo, M. Salmona, D. Ruiz-Molina, A. Badia, et al., Acetylcholinesterase as an amyloid enhancing factor in PrP82-146 aggregation process, Mol. Cell Neurosci. 40 (2009) 217–224.
[12] H. Soreq, S. Seidman, Acetylcholinesterase – new roles for an old actor, Nat. Rev. Neurosci. 2 (2001) 294–302.
[13] R.S. Li, X.B. Wang, X.J. Hu, L.Y. Kong, Design, synthesis and evaluation of flavonoid derivatives as potential multifunctional acetylcholinesterase inhibitors against Alzheimer's disease, Bioorg. Med. Chem. Lett. 23 (2013) 2636–2641.
[14] (a) P. Anand, B. Singh, N. Singh, A review on coumarins as acetylcholinesterase inhibitors for Alzheimer's disease, Bioorg. Med. Chem. 20 (2012) 1175–1180;
(b) S.F. Razavi, M. Khoobi, H. Nadri, A. Sakhteman, A. Moradi, S. Emami, A. Foroumadi, A. Shafiee, Synthesis and evaluation of 4-substituted coumarins as novel acetylcholinesterase inhibitors, Eur. J. Med. Chem. 64 (2013) 252–259.
[15] A. Fallarero, P. Oinonen, S. Gupta, P. Blom, A. Galkin, C.G. Mohan, et al., Inhibition of acetylcholinesterase by coumarins: the case of coumarin 106, Pharmacol. Res. 58 (2008) 215–221.
[16] Z. Radic, P. Taylor, Peripheral site ligands accelerate inhibition of acetylcholinesterase by neutral organophosphates, J. Appl. Toxicol. 21 (Suppl. 1) (2001) S13–S14.
[17] (a) M. Alipour, M. Khoobi, A. Foroumadi, H. Nadri, A. Moradi, A. Sakhteman, et al., Novel coumarin derivatives bearing *N*-benzyl pyridinium moiety: potent and dual binding site acetylcholinesterase inhibitors, Bioorg. Med. Chem. 20 (2012) 7214–7222;
(b) M. Alipour, M. Khoobi, H. Nadri, A. Sakhteman, A. Moradi, M. Ghandi, et al., Synthesis of some new 3-Coumaranone and coumarin derivatives as dual inhibitors of Acetyl- and butyrylcholinesterase, Arch. Pharm. Chem. Life Sci. 346 (2013), http://dx.doi.org/10.1002/ardp.201300080.
[18] M. Khoobi, L. Ma'mani, F. Rezazadeh, Z. Zareie, A. Foroumadi, A. Ramazani, et al., One-pot synthesis of 4H-benzo[b]pyrans and dihydropyrano[c]chromenes using inorganic-organic hybrid magnetic nanocatalyst in water, J. Mol. Catal. A Chem. 359 (2012) 74–80.
[19] F. Cheng, W. Li, Y. Zhou, J. Shen, Z. Wu, G. Liu, et al., admetSAR: a comprehensive source and free tool for assessment of chemical ADMET properties, J. Chem. Inf. Model. 52 (2012) 3099–3105.
[20] G.L. Ellman, K.D. Courtney, V. Andres Jr., R.M. Feather-Stone, A new and rapid colorimetric determination of acetylcholinesterase activity, Biochem. Pharmacol. 7 (1961) 88–95.
[21] M.F. Sanner, Python: a programming language for software integration and development, J. Mol. Graph. Model. 17 (1999) 57–61.
[22] N.M. O'Boyle, M. Banck, C.A. James, C. Morley, T. Vandermeersch, G.R. Hutchison, Open Babel: an open chemical toolbox, J. Cheminform. 3 (2011) 33.
[23] O. Trott, A.J. Olson, AutoDock Vina: improving the speed and accuracy of docking with a new scoring function, efficient optimization, and multithreading, J. Comput. Chem. 31 (2010) 455–461.
[24] E.F. Pettersen, T.D. Goddard, C.C. Huang, G.S. Couch, D.M. Greenblatt, E.C. Meng, et al., UCSF Chimera–a visualization system for exploratory research and analysis, J. Comput. Chem. 25 (2004) 1605–1612.